Surface scattering of small molecules: Theoretical analysis of C_2H_2 scattering from LiF(001)

Ileana Iftimia and J. R. Manson
Department of Physics and Astronomy, Clemson University, Clemson, South Carolina 29634
(Received 13 August 2001; published 13 March 2002)

Calculations with a recently developed theoretical model for molecule-surface scattering are compared with recent high-precision measurements of the scattering of C_2H_2 molecule from a clean, ordered LiF(001) surface. The theory uses a classical treatment of the rotational and translational motion of the molecule, including multiphonon excitations at the surface, while internal vibrational modes of the molecule are treated quantum mechanically. The calculated results for the angular distributions, the scattered intensity as a function of rotational-energy transfer, and final rotational temperatures as a function of incident beam energy are in better agreement with measurements than previous purely classical models. A number of predictive calculations are presented for quantities that can, in principle, be measured.

DOI: 10.1103/PhysRevB.65.125412 PACS number(s): 82.20.Rp, 34.50.Dy, 34.50.Pi

I. INTRODUCTION

Understanding the transfer of energy that occurs in collisions between molecules and surfaces is a question of fundamental importance, and is also essential for predicting the outcomes of processes such as sticking and surface-mediated chemical reactions. Knowledge of molecular scattering is somewhat limited compared with analogous atomic-scattering processes,[1,2] largely due to the greater complexity of molecule-surface interactions. While much of the work on atom-surface collisions has been oriented toward using rare-gas atomic projectiles as a diagnostic tool to determine surface properties, the scattering of molecules is motivated more by its relationship to surface chemical reactions that may occur as a result of the interaction with the substrate or other adsorbates.

In comparison with scattering of atomic projectile, molecular scattering is a much more complicated process because of the internal degrees of freedom of the projectile, such as vibrations and rotations, which can be excited during the scattering process. Thus, much of the literature is concerned with diatomic molecules while data for polyatomic molecules are much more limited. A large number of experiments have been carried out involving NO as the scattering projectile.[3–11] Other experiments used CO,[12,13] HF,[14] HCl,[15] H_2,[16–21] and N_2 (Refs. 22–25) as projectile molecules. Only few larger molecules have also been investigated, for example, CO_2,[26] SF_6,[27] NH_3,[28] and CH_4.[22,29]

This work is motivated by a series of high-precision measurement results[30,31] published for the surface scattering of several molecular species possessing relatively low frequency internal vibrational modes.[29,32,33] Most extensively investigated among these is C_2H_2 scattering from clean, ordered LiF(001).[30] Preliminary analysis of these experiments has been carried out using theories for the classical scattering of rigid molecules, and the initial results have given encouraging quantitative and qualitative agreement with the measured data.[34,35] The purpose of this work is to apply a recently developed theory of mixed classical-quantum scattering to the analysis of the available C_2H_2 data. This theoretical model includes energy and momentum transfers between the surface and projectile for both translational and rotational motions, and internal mode excitation for projectile molecule. The translation and rotation motions are treated in the classical limit for a repulsive surface barrier with an attractive physisorption well. A quantum treatment for internal vibrational mode excitation is used, with extension to arbitrary numbers of internal modes and arbitrary numbers of multiquantum excitations of each mode.

Classical theory should be quite appropriate for describing the translational motion and energy exchange with the surface phonons because C_2H_2 is a large molecule. In fact it is six times heavier than He, for which classical theory has been successfully applied providing the incident energy is greater than about 100 meV.[36] Similarly, for such a high-mass molecule as C_2H_2 the number of rotational quanta transferred in a surface collision will also be large, and a classical treatment is adequate.

The organization of this paper is as follows. In the following section the theoretical model is briefly described and a simple normal-mode analysis for the internal vibrational modes of the acetylene molecule is discussed. In Sec. III the theoretical model is used in calculations, which are then compared with the measured experimental data for angular distributions and final rotational energy states. In Sec. IV a number of predictive calculations is shown for quantities that can, in principle, be measured, while in Sec. V the quantum-excitation probabilities for internal modes are discussed. In Sec. VI the results are discussed and several conclusions are drawn.

II. DESCRIPTION OF THE THEORY

The main theoretical result of the mixed classical-quantum model used here is expressed in terms of a transition rate for scattering from the initial state $\{i\}$ to a final state $\{f\}$. The state $\{f\}$, for example, is specified by $\{\mathbf{p}_f, \mathbf{l}_f, \alpha_{jf}\}$, where $\mathbf{p}_f$ is the final translational momentum of the projectile with corresponding energy E_f^T, $\mathbf{l}_f$ is the final rotational angular momentum with corresponding energy E_f^R, and α_j is the excitation quantum number for the jth internal molecular mode of energy $\hbar\omega_j$. Once this state-to-state transition rate is specified, all measurable quantities can be calculated from it, either by summing over initial and final states that are not measured in a particular experiment or by carrying out the

appropriate averages using the transition rate as the weighting distribution function.

This transition rate, expressed as a summation over all internal modes, has been determined to be[37,38]

$$w(\mathbf{p}_f,\mathbf{l}_f,\mathbf{p}_i,\mathbf{l}_i)=\frac{1}{\hbar^2}|\tau_{fi}|^2\left(\frac{2\pi\hbar^2 v_R^2\beta_T}{\Delta E_0}\right)\left(\frac{2\pi\hbar^2\omega_R^2\beta_T}{\Delta E_0^R}\right)^{1/2}\left(\frac{\pi\hbar^2\beta_T}{(\Delta E_0+\Delta E_0^R)}\right)^{1/2}\exp\left[-\frac{2\mathbf{P}^2v_R^2\beta_T}{4\Delta E_0}\right]$$
$$\times\exp\left[-\frac{2l_z^2\omega_R^2\beta_T}{4\Delta E_0^R}\right]\sum_{\kappa,\kappa'=1}^{N_A}\left\{\exp[i(\mathbf{p}_f\cdot\Delta\mathbf{r}^f_{\kappa,\kappa'}-\mathbf{p}_i\cdot\Delta\mathbf{r}^i_{\kappa,\kappa'})/\hbar]\exp[-W^p_{V,\kappa}(\mathbf{p}_f,\mathbf{p}_i)]\right.$$
$$\left.\times\exp[-W^p_{V,\kappa'}(\mathbf{p}_f,\mathbf{p}_i)]\prod_{j=1}^{N_\nu}\sum_{\alpha_j=-\infty}^{\infty}I_{|\alpha_j|}(b_{\kappa,\kappa'}(\omega_j))\left[\frac{n(\omega_j)+1}{n(\omega_j)}\right]^{\alpha_j/2}\exp\left[-\frac{\mathcal{E}^2\beta_T}{4(\Delta E_0+\Delta E_0^R)}\right]\right\},\qquad(1)$$

where $\beta_T=1/k_BT_S$ with T_S the surface temperature and k_B the Boltzmann constant, and the energy exchange argument is given by $\mathcal{E}=E_f^T-E_i^T+E_f^R-E_i^R+\Delta E_0+\Delta E_0^R+\hbar\Sigma_{s=1}^{N_\nu}\alpha_s\omega_s$. The argument of the modified Bessel function, whose order α_j is the excitation quantum number of the jth internal mode is

$$b_{\kappa,\kappa'}(\omega_j)=\sum_{\gamma,\gamma'=1}^{3}p_\gamma p_{\gamma'}\frac{1}{N_\nu\sqrt{m_\kappa m_{\kappa'}}\hbar\omega_j}$$
$$\times e(^\kappa_j|\gamma)e^*(^{\kappa'}_j|\gamma')\sqrt{n(\omega_j)[n(\omega_j)+1]},\quad(2)$$

where the $e(^\kappa_j|\gamma)$ are the polarization vectors for the γth cartesian component of the κth molecular atom for the jth mode, N_ν is the total number of modes, N_A is the number of atoms of the projectile molecule, and $n(\omega_j)$ is the Bose-Einstein occupation number for the incident molecule with vibrational temperature T_V. In Eqs. (1) and (2) $\mathbf{p}=\mathbf{p}_f-\mathbf{p}_i$ is the scattering momentum and $\mathbf{P}$ is its component parallel to the surface. The translational recoil energy is $\Delta E_0=p^2/2M_c$, where M_c is the substrate molecular mass, and similarly ΔE_0^R is the rotational recoil energy. $\Delta\mathbf{r}_{\kappa,\kappa'}$ is the displacement vector between two molecular atoms, and the Debye-Waller argument for excitation of internal modes is given by

$$W^p_{V,\kappa}(\mathbf{p}_f,\mathbf{p}_i)=\sum_{\gamma,\gamma'=1}^{3}p_\gamma p_{\gamma'}\sum_{j=1}^{N_\nu}\frac{1}{2\hbar N_\nu m_\kappa\omega_j}$$
$$\times e(^\kappa_j|\gamma)e^*(^\kappa_j|\gamma')\{n(\omega_j)+1/2\}.\qquad(3)$$

There are two parameters associated with this theory: v_R is a weighted average of phonon velocities parallel to the surface,[39,40] and ω_R is a weighted average of angular frequencies of the frustrated rotations perpendicular to the surface for the substrate molecules.[37,38] $|\tau_{fi}|^2$ is the scattering form factor and it depends on the interaction potential.

In many cases, such as where the incident molecular energy and the surface temperature are not large compared to the energy of internal molecular vibrational excitations, the expansion of Eq. (1) to only single quantum excitations is sufficient. This expansion is

$$w(\mathbf{p}_f,\mathbf{l}_f,\mathbf{p}_i,\mathbf{l}_i)=\frac{1}{\hbar^2}|\tau_{fi}|^2\left(\frac{\pi\hbar^2\beta_T}{(\Delta E_0+\Delta E_0^R)}\right)^{1/2}\left(\frac{2\pi\hbar^2v_R^2\beta_T}{\Delta E_0}\right)\left(\frac{2\pi\hbar^2\omega_R^2\beta_T}{\Delta E_0^R}\right)^{1/2}\exp\left[-\frac{2\mathbf{P}^2v_R^2\beta_T}{4\Delta E_0}\right]\exp\left[-\frac{2l_z^2\omega_R^2\beta_T}{4\Delta E_0^R}\right]$$
$$\times\sum_{\kappa,\kappa'=1}^{N_A}\exp[i(\mathbf{p}_f\cdot\Delta\mathbf{r}^f_{\kappa,\kappa'}-\mathbf{p}_i\cdot\Delta\mathbf{r}^i_{\kappa,\kappa'})/\hbar]\exp[-W^p_{V,\kappa}(\mathbf{p}_f,\mathbf{p}_i)]\exp[-W^p_{V,\kappa'}(\mathbf{p}_f,\mathbf{p}_i)]$$
$$\times\left\{\exp\left[-\frac{\mathcal{E}_0^2\beta_T}{4(\Delta E_0+\Delta E_0^R)}\right]+\sum_{\gamma,\gamma'=1}^{3}p_\gamma p_{\gamma'}\sum_{j=1}^{N_\nu}\frac{1}{2\hbar N_\nu\sqrt{m_\kappa m_{\kappa'}}\omega_j}e(^\kappa_j|\gamma)e^*(^{\kappa'}_j|\gamma')\right.$$
$$\left.\times\left(n(\omega_j)\exp\left[-\frac{\mathcal{E}_-^2\beta_T}{4(\Delta E_0+\Delta E_0^R)}\right]+[n(\omega_j)+1]\exp\left[-\frac{\mathcal{E}_+^2\beta_T}{4(\Delta E_0+\Delta E_0^R)}\right]\right)\right\},\qquad(4)$$

where the energy arguments are given by $\mathcal{E}_0=E_f^T-E_i^T+E_f^R-E_i^R+\Delta E_0+\Delta E_0^R$ and $\mathcal{E}_{+/-}=E_f^T-E_i^T+E_f^R-E_i^R+\Delta E_0+\Delta E_0^R\pm\hbar\omega_j$. Equation (4) consists of three separate terms within the large curly brackets. The first term is the rate for scattering with no internal mode creation, the term proportional to $n(\omega_j)+1$ gives the single quantum creation rate, and the term proportional to $n(\omega_j)$ is for single quantum annihilation.

The experimental quantity usually measured in a surface scattering process is the differential reflection coefficient $d^3R/d\Omega_f dE_f^T$ giving the fraction of the incident particles that are scattered into a final solid angle of $d\Omega_f$ and energy interval dE_f^T. This is obtained from the transition rate shown in Eqs. (1) and (4) by dividing by the incident flux crossing a plane parallel to the surface and multiplying by the density of available final particle states,

$$\frac{d^3R}{d\Omega_f dE_f^T}(\mathbf{p}_f,\mathbf{l}_f,\alpha_{jf},\mathbf{p}_i,\mathbf{l}_i,\alpha_{ji}) = \frac{L^4}{(2\pi\hbar)^3}\frac{m^2|\mathbf{p}_f|}{p_{iz}}w(\mathbf{p}_f,\mathbf{l}_f,\alpha_{jf},\mathbf{p}_i,\mathbf{l}_i,\alpha_{ji}). \quad (5)$$

Many experiments use a velocity-dependent detector for which a correction must be applied. In the case of a density detector in which the detection probability is inversely proportional to the time of traversal, which is the case for the experiments of interest here,[30] Eq. (5) should be divided by the final molecular translational speed.

The form factor $|\tau_{fi}|^2$ appearing in Eqs. (1) and (4) depends on the form of the interaction potential. In many treatments of inelastic surface scattering the interaction potential is taken to be the repulsive part of the total molecule-surface interaction, which is approximately an exponentially decreasing function of the molecule-surface separation.[2] Thus the form-factor amplitude τ_{fi} appropriate for use here is the transition matrix for the repulsive inelastic interaction. An expression that has been extremely useful, both for multiphonon scattering and for single-phonon studies of atom-surface collisions,[41,42] is an expression given by the distorted-wave Born approximation for an exponentially repulsive potential, first discussed by Jackson and Mott.[43] The Jackson-Mott matrix element, $\tau_{fi}=v_{J\text{-}M}(p_{fz},p_{iz})$ is the matrix element of an exponentially repulsive potential $V(z)=V_0e^{-\beta z}$ taken with respect to its own eigenstates. Defining $q_i=p_{iz}/\hbar\beta$ and $q_f=p_{fz}/\hbar\beta$, it is given by

$$\tau_{fi}=v_{J-M}(p_{fz},p_{iz}) = \frac{\hbar^2\beta^2}{m}\frac{\pi q_i q_f(q_f^2-q_i^2)}{\cosh(\pi q_f)-\cosh(\pi q_i)}\left(\frac{\sinh(\pi q_f)\sinh(\pi q_i)}{q_i q_f}\right)^{1/2}. \quad (6)$$

In the semiclassical limit of a strongly repulsive surface barrier, which here corresponds to $\beta\to\infty$, the Jackson-Mott matrix element becomes[43,44]

$$v_{J\text{-}M}(p_{fz},p_{iz})\to 2p_{fz}p_{iz}/m. \quad (7)$$

The same expression as Eq. (7) is obtained for other potentials in the limit of a strongly repulsive surface barrier, including the Morse potential and a simple Heaviside step potential.

For this work, Eq. (7) was used as the form factor, after modification by the addition of an attractive well. For classical translational motion, such as considered here, the major effects of the adsorption well in the potential are to accelerate the incoming projectiles and to refract them into directions more normal to the surface plane. The acceleration and refraction are independent of the shape of the attractive part of the well, so we have used the simplest approximation, that of a square well. Upon entering the attractive well, the energies are transformed according to $E'^T_q=E^T_q+|D|$, where D is the well depth, but all of this increased energy is associated with the perpendicular motion, hence

$$p'^2_{qz}=p^2_{qz}+2m|D|. \quad (8)$$

The differential reflection coefficient of Eq. (5) is then modified by multiplying by the Jacobian determinant relating energy and solid angle inside and outside of the well.

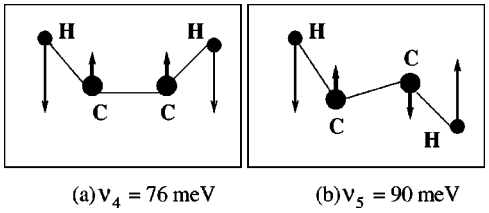

FIG. 1. The two lowest frequency internal vibrational modes for C_2H_2 molecule.

The final quantities to be specified are the polarization vectors for the internal vibrational modes of the C_2H_2 molecule. The only modes of energy small enough to be appreciably excited for incident translational energies of less than 1000 meV of interest here, are the ν_4 and ν_5 bending modes at 76 and 90 meV, respectively. For this we employed a simple ball-and-springs model with two angle-bending restoring springs, one acting at the C-C bonds and the other acting at the H-C bonds. The bond lengths were taken to be $l_{CH}=1.06$ Å and $l_{CC}=1.20$ Å.[45] The ν_4 mode is of even parity in the C and H motion, while the ν_5 mode is of odd parity, as shown in Fig. 1. The two mode frequencies completely specify the angle-bending spring values to be $k_{CH}=5696$ amu meV^2 and $k_{CC}=4180$ amu meV^2. Calculated values of the ν_4 and ν_5 polarization vectors and mode frequencies for C_2H_2 and also for several different isotopic combinations are shown in Table I.

III. COMPARISON WITH EXPERIMENT

The theory reviewed in the preceding section has been compared with a series of experimental data obtained by Francisco *et al.* who have developed a high-resolution experimental apparatus for the scattering of molecules from surfaces.[30] This apparatus is designed to simultaneously study the translational, rotational, and vibrational states of the molecule both before and after collision with the surface. In a high-vacuum chamber, a nearly translationally monoenergetic beam of molecules that is vibrationally and rotationally cold is produced in a supersonic jet. This molecular beam is passed through a laser beam using a multipass geometry, which is used to monitor the incident rotational and vibrational state, and the doppler shift spectra give the molecular translational velocity. Similar detection apparatus is placed in the path of the reflected molecules at a given final

TABLE I. Calculated values of the ν_4 and ν_5 polarization vectors, mode frequencies, and the creation probabilities of the internal-bending-mode quanta for C_2H_2 and also for several different isotopic combinations. P_c is the fractional excitation probability for single quantum creation calculated for incident translational energy $E_i^T = 618$ meV.

Molecule	$h\nu$ (meV)	Polarization vectors				P_c ($\times 10^{-2}$)
${}^1_1H-{}^{12}_6C\equiv{}^{12}_6C-{}^1_1H$	76.00	0.700	−0.010	−0.010	0.700	1.66
	90.00	−0.700	0.100	−0.100	0.700	2.78
${}^1_1H-{}^{12}_6C\equiv{}^{13}_6C-{}^1_1H$	75.70	0.703	−0.010	−0.010	0.711	1.28
	89.20	−0.709	0.107	−0.099	0.690	2.93
${}^1_1H-{}^{12}_6C\equiv{}^{12}_6C-{}^2_1H$	60.45	0.579	0.064	−0.095	0.807	4.37
	85.50	0.974	−0.106	0.097	−0.174	2.61
${}^1_1H-{}^{13}_6C\equiv{}^{12}_6C-{}^2_1H$	60.42	0.567	0.061	−0.098	0.816	4.47
	84.96	0.975	−0.098	0.098	−0.174	2.51
${}^1_1H-{}^{12}_6C\equiv{}^{13}_6C-{}^2_1H$	60.15	0.568	0.067	−0.090	0.815	4.35
	85.15	−0.976	0.105	−0.089	0.166	2.50

angle for measuring the same properties of the scattered molecules. The design of this new apparatus overcomes many of the limitations experienced in previous attempts to study molecule-surface scattering. It provides a full state-to-state scattering capability for many classes of molecular projectiles, and thus allows the possibility of studying a large range of energy and momentum transfers between vibrational modes, rotational states, and phonon exchange with the surface during the scattering process.

The experiments on scattering of C_2H_2 from a clean, ordered LiF(001) surface[30] that we consider here were carried out with an incident molecular beam whose translational energy varied between 90 and 620 meV and energy resolution $\Delta E_i^T/E_i^T$ was better than 10%. The rotational energy of the incident beam was very nearly described by a Maxwell-Boltzmann distribution with a rotational temperature in the range $24 < T_{iR} < 42$ K.[30] The incident angle θ_i was fixed at 60° with respect to the surface normal. The detection apparatus was able, at any given scattering polar angle θ_f in the sagittal plane, to resolve both the translational and the rotational energy of the scattered molecules. Measurements were reported for the total angular distributions as a function of final scattering angle θ_f. Further measurements at fixed values of θ_f determined the scattered intensity as a function of rotational energy, from which a rotational temperature of the scattered beam was extracted through comparison with a Maxwell-Boltzmann function. Values of the final rotational temperatures were reported over the entire translational-energy range of the experiment.

A. Angular distributions

Three experimental angular distributions taken at different incident energies are shown in Fig. 2 and compared with calculations carried out using Eq. (5). The experimental data are exhibited as solid lines for the three incident energies (a) $E_i^T = 110$ meV, (b) $E_i^T = 275$ meV, and (c) $E_i^T = 618$ meV as shown. The experiment exhibits an increasingly narrowing angular distribution with increasing incident translational energy, and simultaneously there is substantial supraspecular shift of the most probable intensity, with the 110-meV distribution peaking at an angle approximately 10° smaller than the 60° specular position and the largest energy peaking at nearly 10° greater than the specular position. At the two larger energies there is negligible intensity scattered with very large total scattering angles, and essentially no intensity scattered backward into the quadrant of the incident beam.

The calculations shown as long dashed curves with different symbols in Fig. 2 were carried out using the differential reflection coefficient of Eq. (5) using an attractive well with a well depth of $|D| = 90$ meV. The incident beam was in the vibrational ground state, had a rotational temperature of 30 K, and was averaged over all rotational and spatial orientations before collision. The differential reflection coefficient, at each angle, was summed over all final translational, rotational, and vibrational states as well as spatial orientations of the molecule.

Several parameters needed to be determined. One parameter is the effective surface phonon velocity v_R, which is expected to be of the order of, or smaller than, the Rayleigh velocity for LiF(001), which is approximately 4000 m/s.[46,47] In this study v_R was given values less than Rayleigh velocity, and was found to be dependent on the incident energy, but to a significantly lesser degree than in previous

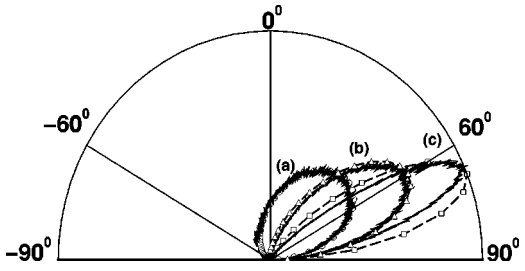

FIG. 2. Polar plots of the measured angular distributions for the scattering of C_2H_2 by LiF(001); (a) $E_i^T = 110$ meV, (b) $E_i^T = 275$ meV, and (c) $E_i^T = 618$ meV, the incident angle is in each case $\theta_i = 60°$ as shown by the solid straight line. The solid lines are the experimental data and the long dashed curves with circle (a), triangle (b), and square (c) symbols are the calculations.

calculations.[34,35] The best fits were obtained with $v_R = 300$ m/s for the lowest energy $E_i^T = 110$ meV, $v_R = 600$ m/s for $E_i^T = 275$ meV, and $v_R = 1000$ m/s for $E_i^T = 618$ meV. The value of the weighted average rotational velocity was chosen to be $\omega_R = 2 \times 10^{10}$ s^{-1} for all calculations presented in this paper. The results also depend on an effective crystal mass for the surface LiF molecules. To obtain the fit in Fig. 2, a value of effective crystal mass $M_c = 77.8$ amu was used, which is three times the total mass of a LiF molecule. This is the same effective crystal mass used in a previous study with a much less refined scattering model.[34] The need for an effective crystal mass larger than that of the LiF molecule seems to indicate that the incoming C_2H_2 projectile is typically colliding with more than one surface LiF molecule.

The theoretical calculations agree rather well with the measurements for these angular distributions. The well in the potential broadens the angular distribution somewhat at lower incident-beam energies, but has little effect for incident energies larger than the well depth.

These calculations indicate that the rotational transfers have a much less significant effect on the shapes of the angular distributions than the phonon-energy transfer, and the internal molecular-vibrational states play little role. This opinion is confirmed by other calculations that have been carried out using cruder models of the rotational excitations and no internal vibrational excitation.[34,35] However, the present calculations agree with the data using a much smaller range of the v_R parameter as the incident energy increases. Thus it appears that the dominant process involved in creating the shapes of the angular distributions is large-number multiple-phonon transfer at a collision with the smoothly varying repulsive part of the potential.

B. Final intensity as a function of rotational energy

Figure 3 shows, at four different incident energies, the measured and calculated scattered intensity as a function of rotational energy for an incident angle $\theta_i = 60°$. The incident energies are written on each graph, and the final angle is, for each incident energy, the position of the maximum in the angular distribution (see Fig. 2). The measured values[30] are shown as experimental points and the calculations are the solid and long dashed curves as explained below. The calculated quantity is the differential reflection coefficient of Eq. (5) averaged over an initial Maxwell-Boltzmann distribution of rotational states with a temperature $T_{iR} = 30$ K as for the calculations of the angular distributions. It is averaged over all orientations of the initial and final angular momenta of the projectile molecule, summed over final translational energies, and averaged over all angular orientations of incident and scattered molecule. The well depth is taken to be $|D| = 90$ meV and the values of v_R were chosen to be the same as those used for the angular distributions shown in Fig. 2, i.e., when the incident energy was not the same as in one of the cases in Fig. 2 the v_R value was chosen by linear interpolation. The calculations using a crystal mass M_c equal to the total mass of a LiF molecule, which is labeled as $mf = 1$, are shown as solid curves in Fig. 3 and the agreement

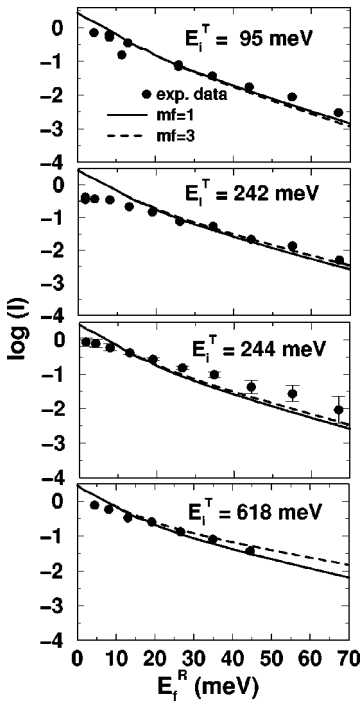

FIG. 3. Logarithmic plots of the scattered intensity as a function of final rotational energy for C_2H_2 scattering from LiF(001). The incident angle is $\theta_i = 60°$ and the final angle is, for each incident energy, at the maximum in the angular distribution. The experimental measurements are shown as data points and the calculations, with $|D| = 90$ meV, are shown as a solid curve for an effective mass equal to that of LiF ($mf = 1$) and as a long dashed curve for an effective mass three times larger ($mf = 3$).

with the data is good. The long dashed curves show similar calculations with an effective crystal mass three times that of LiF, $mf = 3$, and in this case the agreement with data is not so good.

In these logarithmic plots, the experimental points, to a reasonable approximation, can be fit to a straight line although the straight line has a different slope depending on incident energy, which might indicate that the final rotational states are distributed according to a Maxwellian distribution with a different rotational temperature at each incident energy. The calculations do not correspond completely to such an equilibrium-distribution interpretation since they are slightly curved at small E_f^R, although they tend to become relatively straight for large E_f^R.

C. Final rotational temperature versus incident translational energy

In Fig. 4 the experimental data points shown with error bars are the measured final rotational temperatures as functions of incident translational energy E_i^T.[30] These rotational temperatures are extracted from a series of plots such as in Fig. 3 by fitting the experimental data to a straight line, in which case the slope of the line gives the temperature of the corresponding Maxwell-Boltzmann distribution. The final calculated rotational temperatures were determined by making a least-squares fit to a straight line over the range 8

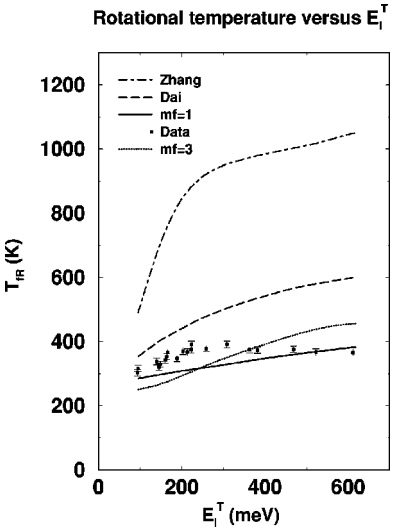

FIG. 4. Incident-energy dependence of the final rotational temperature of C_2H_2 scattered from LiF(001) for $\theta_i=60°$ and θ_f at the maximum in the respective angular distributions. The experimental measurements are shown as data points with error bars and the present calculations are shown as the solid and dotted curve, respectively, for effective masses, mf, equal to one and three times that of LiF. The dash-dotted and long dashed curves show two earlier calculations for rigid molecules, as explained in the text.

$<E_f^R<90$ meV, essentially the same energy range over which the measurements were taken. All parameters in these calculations are the same as those used in Fig. 3, including the use of a well depth of $|D|=90$ meV. The straight-line curve in Fig. 4 is a result of the calculation described above with $mf=1$, and the dotted curve is for $mf=3$.

The two other curves plotted in Fig. 4 are based on classical theories, which consider that C_2H_2 is a small, rigid molecule[34,35] with no internal degrees of freedom. The dash-dotted line[34] is obtained using a model in which rotational excitations are described by the incoming acetylene interacting with a surface of discrete LiF molecules in a thermal distribution of states. The long dashed line[35] is for a rigid molecular model in which the rotational excitations are caused by a smoothly varying repulsive potential, which gives the correct rotational angular momentum conservation, i.e., angular momentum is conserved only in the direction perpendicular to the surface, as in the model used here. These two earlier classical calculations are only in qualitative agreement with the experimental data, although the curves have the same general shape as the experiment—they both overestimate the effective intensity for rotational excitation.

The present calculations, especially those with $mf=1$, are in a much better agreement with the experimental data. Since the present theoretical model differs from the earlier rigid-molecule model[35] mainly by the inclusion of the internal bending-mode degrees of freedom, the reduction in calculated rotational temperatures (or alternatively, the better agreement of the rotational intensities of Fig. 3) is clearly due to the internal modes. The possible importance of the internal modes had been suggested earlier.[30] The effect of the internal bending modes does not appear to be caused by large

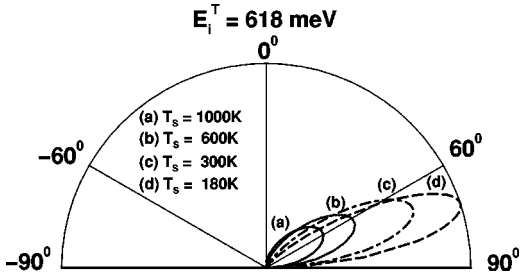

FIG. 5. Surface-temperature dependence of the angular distribution for C_2H_2 scattering from LiF(001) for several different surface temperatures as shown, $E_i^T=618$ meV.

probabilities of excitation, or multiple quanta of excitation of these modes. In fact, as is shown below, this model predicts relatively small probabilities for single quantum internal-mode excitation, and negligible probabilities for multiple quantum overtone excitations over the energy range of interest. Instead, the reduction of intensity, as compared to rigid-molecule models, appears to be a result of the phase-interferences introduced by the presence of discrete vibrational channels. These phase interference terms are evident in Eq. (1) or (4) in the exponential phase factors associated with the orientational position of the molecule during the collision process. If it were possible to observe molecules scattered in a particular orientation relative to the surface plane, then these phase factors would cause structure to appear in the scattered intensity. Averaging over all orientations, as is done by the detector, makes this underlying structure impossible to observe; however, the effect of this quantum interference from the vibrational modes is to give an overall reduction to the effective final rotational temperatures.

IV. FURTHER CALCULATIONS

Presented in this section are a number of calculations of measurable quantities for which at present there is no experimental data available. All calculations were made for the case of C_2H_2 scattering from LiF(001), and the relationship of the results of each of these calculations to the relevant features of the interaction potential and surface characteristics is discussed.

A. Temperature dependence of angular distributions

In previous work on the classical scattering of heavy-mass rare-gas atoms from metal surfaces under classical scattering conditions at energies similar to those in the present work, it has been shown that the temperature dependence of the energy-resolved spectra and angular distributions could be related to the average corrugation height of the atomic-scale roughness of the surface.[48–50] Figure 5 shows the calculated angular distributions at the energy of 618 meV for several surface temperatures, ranging from $T_S=180$ to 1000 K. The incident angle is 60° and all parameters were chosen to be the same as used in the angular distribution presented earlier in Fig. 2.

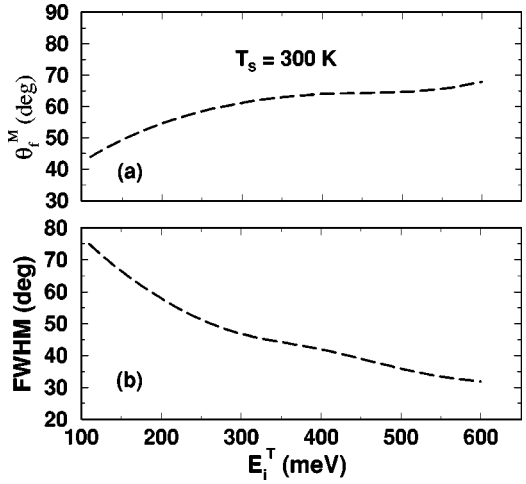

FIG. 6. Incident-energy dependence of the polar-angle position of the angular-distribution maximum (a) and of the angular-distribution width (b) for C_2H_2 scattering from LiF(001) for $T_S = 300$ K.

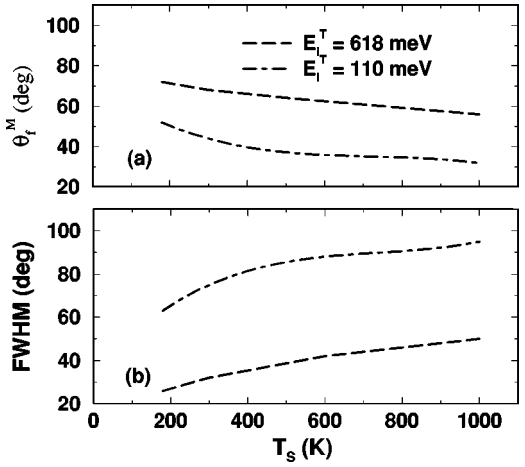

FIG. 7. Surface-temperature dependence of the polar-angle position of the angular-distribution maximum (a) and of the angular-distribution width (b) for C_2H_2 scattering from LiF(001) for $E_i^T = 110$ and 618 meV, as shown.

Clearly, with increasing temperature the angular distribution becomes broader and its most probable intensity decreases. This is an immediate effect of unitarity, i.e., the principle that the number of incident particles equals the number of scattered particles. As the temperature increases, the number of possible final inelastic channels increases causing the angular distribution to broaden, and concomitantly the maximum intensity will decrease in order to preserve the total number of scattered particles.

There is also a shift of the most probable intensity in the subspecluar direction with increasing temperature. This appears to be the result of two effects: (1) the average final translational energy of the scattered particles is larger at higher temperatures and (2) this scattering model contains correct conservation of parallel momentum, i.e., although the parallel momentum of a scattered particle may differ greatly from that of the incident beam because many phonons have been transferred, for each phonon exchange only momentum parallel to the surface is conserved. Thus at higher temperatures the average momentum normal to the surface is enhanced with respect to the parallel momentum, leading to the subspecular shift.

B. Positions and widths of the angular distributions

The behavior of the most probable intensities and the widths of the angular distributions is more clearly shown in Figs. 6 and 7. Panel (a) of Fig. 6 shows the incident-translational-energy dependence of the most probable intensity of the in-plane angular distribution, with the surface temperature at 300 K and all parameters the same as the calculations shown in Fig. 5 above. It is seen that the polar-angle position of the most probable intensity undergoes a supraspecular shift with increasing incident energy. This is expected, again as a result of the parallel momentum conservation built into this theory. At these incident energies, the energy of the incident beam is considerably larger than the surface temperature, i.e., using a $k_B T_S$ conversion, a surface temperature of 300 K is approximately 27 meV. Thus at these relatively elevated incident energies compared to the temperature, the incident molecules lose total energy to the surface on average and this, combined with the necessary parallel momentum conservation, means that the reduction of the average final normal momentum is enhanced compared to that of the average parallel momentum with increasing incident energy, resulting in a supraspecular shift of the outgoing angular-distribution lobe. The same physical argument would predict a decrease in the width of the angular distributions with increasing incident energy, and this behavior is demonstrated in Fig. 6(b) where the full width at half maximum is plotted versus E_i^T.

Panel (a) of Fig. 7 shows the decrease in polar-angle position of the most probable intensity of the angular-distribution lobe as a function of surface temperature for the two incident energies, $E_i^T = 110$ and 618 meV. The subspecular shift discussed above in Sec. IV A above is clearly evident. The increasing width with surface temperature is shown in panel (b) of Fig. 7. All parameters shown in Figs. 6 and 7 are the same as in Fig. 5.

C. Average final rotational energy "in-plane"

In this section properties of the final rotational energy are presented when its average is taken only for "in-plane" scattering angles, i.e., for scattering in the sagittal plane, which includes the incident beam and normal to the surface. Figure 8 gives the dependence on scattering angle (a) and incident energy (b) of the average "in-plane" final rotational energy E_f^R for C_2H_2 scattering from LiF(001). In Fig. 8(a) $E_i^T = 618$ meV and $T_S = 180$ and 300 K as shown and E_f^R is plotted against θ_f. In Fig. 8(b) θ_f is taken, for each incident energy, at the maximum in the angular distribution and E_f^R is plotted as a function of E_i^T. In all these calculations, made with an attractive potential well of depth $|D| = 90$ meV, the incident angle was chosen $\theta_i = 60°$, and v_R was obtained by linear interpolation as explained in Sec. III B above. Also, a

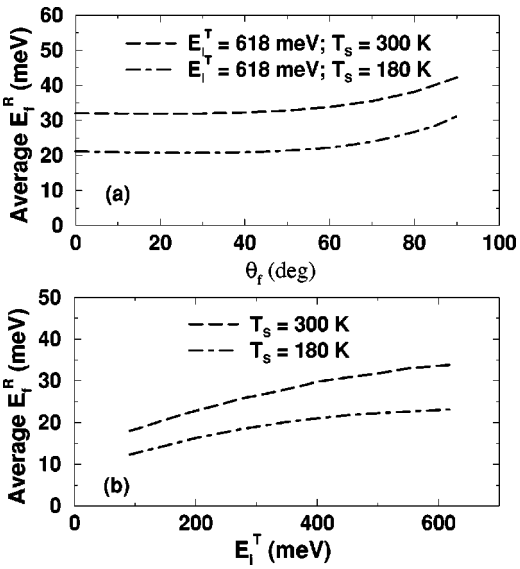

FIG. 8. Scattering-angle (a) and incident-energy (b) dependence of the average final rotational energy for C_2H_2 scattering from LiF(001). (a) $T_S=180$ and 300 K, $E_i^T=618$ meV and (b) $T_S=180$ and 300 K, and the final angle is, for each incident energy, at the maximum in the angular distribution.

crystal mass $M_c=77.8$ amu, $mf=3$, was used. The average final rotational energy is seen to be relatively constant at all angles in the angular distribution, but increases with increasing incident energy.

D. Three-dimensional average final rotational and translational energies

Also readily calculatable are full three-dimensional averages of final rotational and translational energy. Figure 9 shows the three-dimensional average final rotational and translational energies as functions of surface temperature for two incident energies $E_i^T=380$ and 618 meV, with an incident angle of 60°. In these calculations, made without a potential well in front of the surface, all other parameters are the same as those used in Sec. IV C above. The average final rotational energy increases with the surface temperature. The final translational energies show very little change or even a

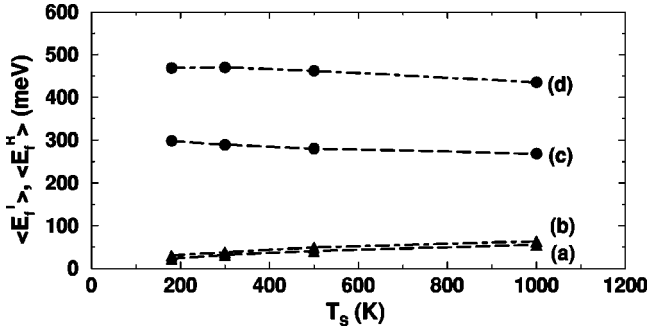

FIG. 9. Surface-temperature dependence of the three-dimensional average final rotational and translational energies. (a) $\langle E_f^R \rangle$ for $E_i^T=380$ meV, (b) $\langle E_f^R \rangle$ for $E_i^T=618$ meV, (c) $\langle E_f^T \rangle$ for $E_i^T=380$ meV, and (d) $\langle E_f^T \rangle$ for $E_i^T=618$ meV.

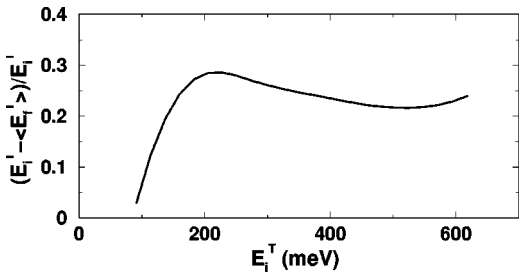

FIG. 10. The fractional energy loss as a function of initial translational energy for $T_S=300$ K.

small decrease with increasing surface temperature, even up to $T_S=1000$ K. The small change is due, as explained above, to the very large incident energy in comparison to the surface temperature. The fact that there is a small decrease with T_S appears to be the result, not only of the enhanced probability of rotational excitation, but also because of creation of internal molecular-vibrational quanta as discussed below in Sec. V, with the energy required for internal-mode excitation subtracted from the translational energy.

The average final translational energies show a significant loss as compared to the incident energy, indicating energy deposited into the surface. This is shown in Fig. 10 which gives the fractional energy loss $(E_i^T-\langle E_f^T \rangle)/E_i^T$ as a function of initial energy, for $T_S=300$ K. It is seen that the fractional energy loss is a rapidly increasing function of the incident energy for $E_i^T<200$ meV after which the average final energy is a relatively constant fraction of the incident energy, as would be predicted by simple kinematical two-body collision models.

E. Rotational energy and recovery energies

In this section the dependence of the final rotational energy on incident rotational energy, and on other incident conditions is considered. In general, it is found that for an incident beam in a given rotational-energy distribution with average energy E_i^R, the final average rotational energy E_f^R is an increasing function of E_i^R, but increases more slowly, i.e., the slope dE_f^R/dE_i^R is positive but less than unity. For E_i^R smaller than the incident translational energy, the final rotational energy E_f^R is usually found to be larger than E_i^R, while as E_i^R increases, eventually a point is crossed where E_i^R becomes greater than E_f^R. This point can be called the ''recovery energy'' in analogy with the definition of a ''recovery temperature'' in the study of gas-surface interactions.

The ''recovery temperature'' is defined as the temperature at which no energy is transferred between the gas and a surface when an incident beam scatters. If a well-defined incident beam of atoms or molecules with energy E_i^T strikes the surface, the average final translational energy $\langle E_f^T \rangle$ can be larger or smaller than E_i^T depending on the surface temperature. The recovery temperature is defined as the temperature at which $E_i^T=\langle E_f^T \rangle$. In the same manner, a ''rotational recovery energy'' E_R can be defined as the point at which $E_i^R=\langle E_f^R \rangle \equiv E_R$.

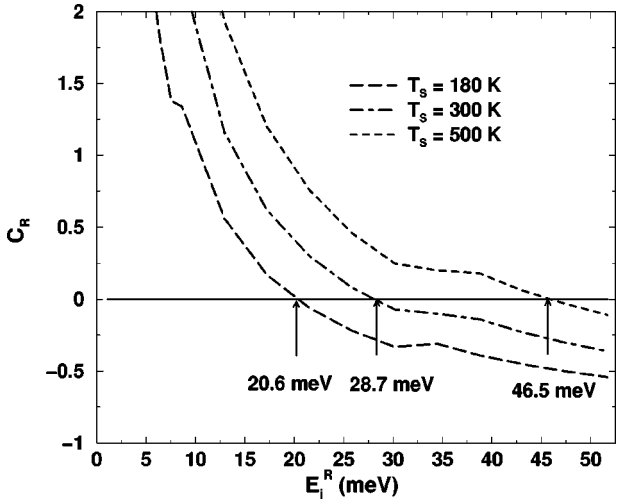

FIG. 11. The relative rotational-energy transfer as a function of incident rotational energy for several different surface temperatures. The incident translational energy is $E_i^T=110$ meV, and $T_S=180$, 300, and 500 K. The recovery energies at each surface temperature are marked.

The existence of a rotational recovery energy is illustrated in Fig. 11 where the relative rotational-energy transfer $C_R=(\langle E_f^R\rangle-E_i^R)/E_i^R$ is plotted as a function of E_i^R. The parameters used in these calculations correspond to those of the best fit (solid curve) in Fig. 4. The incident translational energy is $E_i^T=110$ meV, $\theta_i=60°$, and three surface temperatures $T_S=180$, 300, and 500 K are shown. The final angle is, for each incident energy, the position of the maximum in the angular distribution (see Fig. 2). The final average rotational energy $\langle E_f^R\rangle$ is determined from the intensity versus rotational-energy distributions such as in Fig. 3, just as was done to obtain the rotational temperatures shown in Fig. 4. It is seen that the rotational recovery energies depend strongly on surface temperature.

The dependence of E_R on surface temperature is shown in Fig. 12 for the two incident translational energies $E_i^T=110$ and 618 meV, other parameters being the same as in Fig. 11. The recovery temperature is a rather strongly increasing function of T_S, indicating that the temperature plays a large role in rotational-energy transfers.

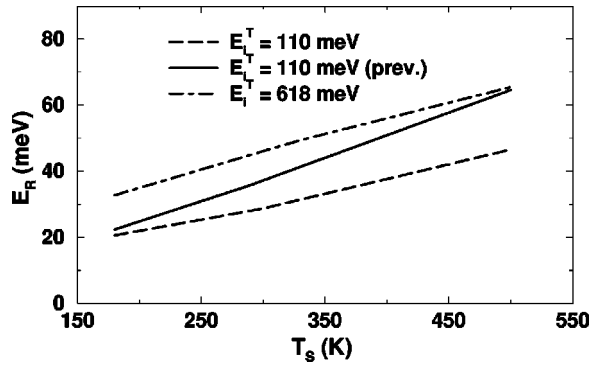

FIG. 12. The rotational recovery energy versus surface temperature for $E_i^T=110$ meV (long dashed curve) and 618 meV (dash-dotted curve). The solid curve gives the result for $E_i^T=110$ meV for a simpler model of a surface of discrete molecules.[34]

Simple models of rotational transfer in molecular collisions do not appear to explain the behavior observed in Figs. 11 and 12. For example, a simple kinematical model of the collision process is the textbook problem of determining the final rotational energy as a function of initial rotational energy by simultaneously solving the equations of conservation of linear momentum, angular momentum, and total energy for a classical two-molecule collision. For the specified initial and final conditions of Figs. 11 and 12 such a model actually predicts that the final rotational energy of the projectile will be a decreasing function of $\langle E_i^R\rangle$, quite the contrary of what is found with the present dynamical model.

A model that is somewhat more sophisticated than the above simple kinematical two-molecule collision is to consider the dynamical interaction of the incoming projectile with a surface of discrete molecules with a temperature T_S.[34] Calculations of the rotational recovery energy for this simpler model are also shown in Fig. 12 as a solid line for the incident translational energy $E_i^T=110$ meV. This model clearly gives E_R values much larger than the present calculations, consistent with the much larger values of T_f^R exhibited by the same model in Fig. 4 above.

V. QUANTUM EXCITATION PROBABILITIES FOR INTERNAL MODES

It is of interest to discuss the predicted probabilities for excitation of internal vibrational modes of C_2H_2 using the present scattering model. For incident energies less than 1 eV our calculations show that the C-C stretch mode at an energy of 244.7 meV, and the two C-H stretch modes at energies of 407.8 and 418.3 meV are negligibly excited. Over the incident-energy range of roughly $100<E_i^T<600$ meV considered here it was found that only single quantum creation of internal modes was a significant process. Multiple quantum overtone creation is found to be smaller than single quantum creation by several orders of magnitude, and single quantum annihilation for such a vibrationally cold incident beam is completely negligible. This simplifies the calculation of the vibrational excitation probabilities because only the single quantum creation events need to be considered. They are calculated as follows. The single quantum terms are identified in the transition rate of Eq. (4) as those proportional to $n(\omega_j)+1$, where $n(\omega_j)$ is the Bose-Einstein probability and ω_j is the mode frequency. For example, given a fixed incident energy, incident angle, and final angle, the probability of single quantum creation of the jth mode is obtained by evaluating the $n(\omega_j)+1$ term in Eq. (4) and summing over all other initial and final variables such as the angular momentum and final translational energy. Dividing this result by the same summation applied to the total transition rate of Eq. (4) gives the relative probability of single quantum excitation for the given fixed incident and final conditions.

The results of these calculations led to several interesting general observations.

(1) Probabilities for excitation of the ν_4 and ν_5 modes appear to be readily measurable. Typical excitation probabili-

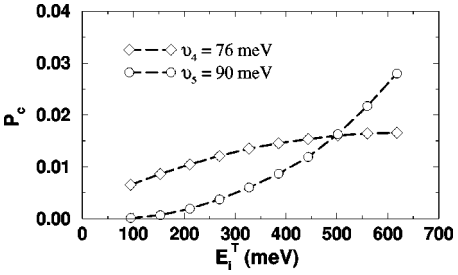

FIG. 13. The relative probability P_c to create a quantum as a function of incident energy for $T_S=300$ K and for a fixed incident and final angle $\theta_i=\theta_f=60°$. The long dashed curves with unfilled diamond and circle symbols show the calculations for the ν_4 and ν_5 modes, respectively.

ties for the ν_4 and ν_5 modes rapidly rose from the creation thresholds to approximately 1.6% and 2.8%, respectively, for incident energies of order $E_i^T \approx 600$ meV.

(2) As mentioned above, since the temperature of the incident beam is very small compared to the lowest C_2H_2 vibrational-mode frequencies, annihilation was completely negligible.

(3) The symmetry of the C_2H_2 molecule seems to be important in the excitation process of the internal vibrational modes. The ν_4 mode is a symmetric vibration, with the two H atoms vibrating in opposition to the two C atoms as seen in Fig. 1. The ν_5 mode, on the other hand, is antisymmetric and its excitation probability was found to be smaller than that for the ν_4 mode over the incident-energy range of roughly $100<E_i^T<500$ meV. The cause of this difference appears to be the quantum-phase cancellation resulting from the position-dependent phase factors apparent in the transition rate of Eq. (4). The antisymmetry gave rise to destructive quantum interference, while the symmetric ν_4 mode has

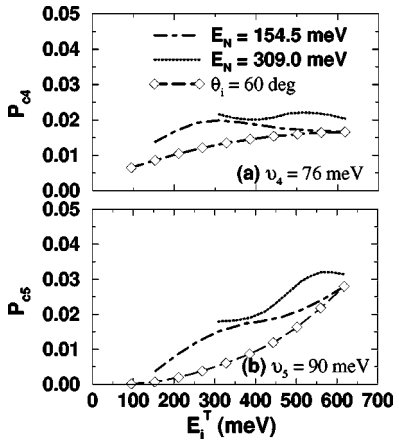

FIG. 14. The relative probability P_c to create a 76-meV ν_4 (a) and a 90-meV ν_5 (b) quantum, as a function of incident energy, for $T_S=300$ K. The long dashed curves with unfilled diamond symbols are calculated for a fixed incident angle $\theta_i=60°$. The dash-dotted curves are calculated for a fixed value of the normal energy $E_N=154.5$ meV by varying the incident angle simultaneously with the incident energy. The dotted curves are for fixed $E_N=309$ meV.

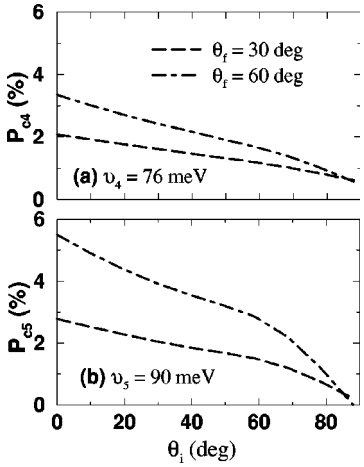

FIG. 15. The relative probability P_c to create a 76-meV ν_4 (a) and a 90-meV ν_5 (b) quantum, as a function of incident angle, for fixed $E_i^T=618$ meV and fixed θ_f, for $T_S=300$ K. The dash-dotted curves are for $\theta_f=60°$ and the long dashed curves are for $\theta_f=30°$.

much more constructive interference during the collision process.

(4) Isotope substitution in acetylene breaks the symmetry of both the ν_4 and ν_5 modes. Replacement of one H atom by deuterium (D) slightly decreases the excitation probability of the ν_5 mode and enhances more than 2.5 times that of the ν_4 mode. However, replacing one of the $^{12}_6$C atoms with a $^{13}_6$C has a relatively small effect on excitation probabilities of the ν_4 and ν_5 modes.

(5) An investigation of the excitation probability as a function of total incident translational energy and as a function of the incident energy associated with motion normal to the surface reveals no indication that the normal energy is a more important predictor of internal-mode excitation than the total energy.

All of the above properties are illustrated by the calculations shown in the following graphs of Figs. 13–15. In all the calculations presented in these plots, $|D|=0$ meV and all other parameters were chosen to be the same as for the angular distributions of Fig. 2 above.

Figure 13 gives the relative probability to create a quantum as a function of incident energy E_i^T for $\theta_i=\theta_f=60°$. The long dashed curves with open diamond and circle symbols show the calculations for ν_4 and ν_5 mode, respectively. The probabilities are seen to rapidly increase above the threshold energy of 76 meV for the ν_4 mode and 90 meV for the ν_5 mode, and at the highest incident energy roughly 5% of the scattered molecules become vibrationally excited. For higher energies the probability of the ν_5 mode increases more abruptly and for $E_i^T \geqslant 500$ meV its intensity becomes somewhat higher than that of the ν_4 mode.

The question of the importance of the ''normal incident energy'' relative to that of the total incident energy is addressed in Figs. 14(a) and 14(b) for the ν_4 and ν_5 modes, respectively. The long dashed curves with open diamond symbols give the relative probability to create a quantum as a function of incident energy E_i^T, for $\theta_i=\theta_f=60°$, as in Fig.

13 above. The dash-dotted curves show calculations with fixed ''normal energy'' $E_N = 154.5$ meV. This is accomplished by varying the incident angle simultaneously with the incident energy so that $E_N = E_i^T \cos^2(\theta_i)$ remains constant. The dotted curves are similar, except when calculated for $E_N = 309$ meV. If the vibrational-mode excitation depended only on the ''normal energy'' then these latter two curves should be constants as a function of total incident translational energy. Instead, their behavior appears similar to that for the corresponding fixed incident beam, even though their shape is somewhat different. This indicates that there seems to be no particular importance attached to the ''normal energy'' in the process of internal-mode excitation.

Another way of examining the internal-bending-mode excitation is shown in Fig. 15, which gives the ν_4 (a) and the ν_5 (b) probability as a function of incident angle for a fixed final angle and a fixed initial translational energy of $E_i^T = 618$ meV. Two curves are shown for the two final angles, $\theta_f = 30°$ and $60°$. This figure shows that there is significant angular variation in the vibrational excitation probability as a function of incident angle. For detection at off-normal final polar angles, the excitation probability decreases if the incident angle increases, becoming very small at grazing incidence.

As briefly mentioned above, broken symmetry due to isotopic substitution in the C_2H_2 molecule can give a small decrease of the ν_5-mode probability and an enhancement of the ν_4-excitation probability. This is shown in Table I, which gives a list of several different possible isotopic substitutions and the excitation-probabilities P_c. The excitation probability calculations were carried out for an incident energy $E_i^T = 618$ meV and $\theta_i = \theta_f = 60°$. It is seen that replacing one of the $^{12}_{6}$C atoms with a $^{13}_{6}$C has a small effect of both probabilities for excitation of the ν_4 and ν_5 modes. However, replacing an H atom with a D enhances the ν_4 mode. Therefore, the ν_4 probability increases more than 2.5 times to approximately 4.37% of the total incoming beam, and the ν_5-mode probability slightly decreases to approximately 2.61% of the total incoming beam. The main reason for this behavior appears to be the considerably larger decrease in energy of the ν_4-mode frequency upon H to D substitution.

VI. CONCLUSIONS

The work reported in this paper uses a relatively straightforward molecular-scattering model to analyze recent data for the scattering of acetylene at hyperthermal energies from a clean and ordered LiF(001) surface.[30] In this theoretical model the translational motion of the projectile molecules are treated classically within a multiphonon-transfer formalism, which preserves the correct conservation of momentum parallel to the surface for each phonon transfer. Similarly, the rotational motion of the molecule is treated classically, also with the correct conservation of angular momentum in the direction perpendicular to the surface. Excitations of internal vibrational modes of the molecule are treated quantum mechanically within a semiclassical theory. All three mechanisms are combined within the separability limit, which means that each process transfers energy self-consistently taking into consideration the energy already transferred by the other processes. The theoretical model is expressed in terms of a closed-form analytic expression for single state-to-state molecular collisions with the surface, which is a very useful property because it enables ready visualization of the expected responses of the translational, rotational, and vibrational distributions of final particles as functions of surface temperature, substrate properties, and other features of the interaction potentials.

The measured experimental data for C_2H_2 scattering from LiF(001) consists of total angular distribution lobes for several incident translational energies, intensity measurements as a function of final molecular-rotational energy, and effective rotational temperatures of the scattered molecules as a function of the incident translational energy. The present theoretical model was used to calculate all of these quantities as well as to make predictive calculations of several other properties of the scattered beam that could be measured.

Good agreement was found between the calculated and measured angular-distribution lobes. Calculations with this model, and comparisons with other simpler models for molecular scattering, indicate that rotational and vibrational transitions play a relatively minor role in producing the shape of the angular-distribution lobes. The angular distributions appear to be formed mainly by classical multiphonon exchange with the surface. Additional calculations show that the phonon-transfer mechanism produces very characteristic behavior of the angular distributions as a function of increasing incident translational energy or surface temperature. With increasing incident energy, the lobes become narrower in width and the lobe maximum undergoes a supraspecular shift in position, in agreement with the available measurements. With increasing surface temperature, the calculations predict that the lobe becomes broader in width while the maximum lobe intensity decreases. At incident translational energies that are small compared to the well depth, the calculated angular-distribution lobes become much broader.

Measurements for the scattered C_2H_2 were made for the intensity as a function of rotational energy. These intensities were found to decay approximately exponentially with rotational energy and, when compared to a Maxwell distribution, could be assigned an effective rotational temperature. Our calculations indicated that the intensity decreased faster than exponentially for very small rotational energies, but over the range that the experiments were measured, relatively good agreement with the intensity versus rotational energy plots was obtained.

The effective rotational temperatures were measured as a function of incident translational energy, and when compared with similar effective rotational temperatures extracted from the calculations, the agreement with the data was good. However, calculations of effective rotational temperatures with earlier and simpler theoretical models using rigid molecules produced effective rotational temperatures that were too large and were only in qualitative agreement with experiment.[34,35] The reason for this earlier lack of agreement is revealed by the present calculations, which include the possibility of excitation of internal degrees of freedom. Although internal-mode excitation probabilities are relatively

small at the incident translational energies of interest here, the quantum-interference effects arising from excitation of internal modes restrict the channels for final scattering. This appears to partially confirm earlier predictions that quantum excitation of internal degrees of freedom was playing a significant role in the values of final effective rotational temperatures.[30]

At the largest incident translational energies of around 600 meV used in the C_2H_2 scattering experiments, the theoretical model predicts a total excitation probability for internal bending modes of approximately 3%–5%. The bond stretching modes have a vibrational energy that is too large to be significantly excited at these incident energies. The excitation probability of the antisymmetric ν_5 mode at 90 meV is smaller than that of the ν_4 mode at 76 meV over a large energy range of roughly $100<E_i^T<500$ meV, in part because of its larger energy, but mainly because of the destructive quantum interference due to its odd vibrational symmetry. Breaking the symmetry through isotopic substitution of a deuterium atom for one of the hydrogen atoms in C_2H_2 enhances the ν_4 intensity and slightly decreases the ν_5 intensity.

The comparisons of theory with experiment shown in this paper show that the present theoretical models can be useful in predicting the translational, rotational, and vibrational behavior in molecule-surface scattering experiments. The fact that the theoretical state-to-state scattering probability can be expressed in terms of analytic, closed-form equations makes it particularly simple to show how individual measurements can be tailored to probe particular aspects of the interaction potential and the energy-transfer processes.

ACKNOWLEDGMENTS

We would like to thank R. E. Miller, A. Wight, J. Dai, and H. Zhang for helpful discussions. This work was supported by the National Science Foundation under Grant No. DMR-0089503 and by the Department of Energy under Grant No. DE-FG02-98ER45704.

[1] J. P. Toennies, in *Surface Phonons*, edited by W. Kress and F. W. de Wette, Springer Series in Surface Science, Vol. 21 (Springer, Heidelberg, 1991), p. 111.
[2] *Helium Atom Scattering from Surfaces*, edited by E. Hulpke, Springer Series in Surface Science (Springer, Berlin, 1992).
[3] A. W. Kleyn, A. C. Luntz, and D. J. Auerbach, Phys. Rev. Lett. **47**, 1169 (1981).
[4] G. D. Kubiak, J. E. Hurst, H. G. Rennagel, G. M. McClelland, and R. N. Zare, J. Chem. Phys. **79**, 5163 (1983).
[5] C. T. Rettner, J. Kimman, and D. J. Auerbach, J. Chem. Phys. **94**, 734 (1991).
[6] D. C. Jacobs, K. W. Kolasinski, S. F. Shane, and R. N. Zare, J. Chem. Phys. **91**, 3182 (1989).
[7] H. Vach, J. Häger, and H. Walther, Chem. Phys. Lett. **133**, 279 (1987).
[8] G. M. McClelland, G. D. Kubiak, H. G. Rennagel, and R. N. Zare, Phys. Rev. Lett. **46**, 831 (1981).
[9] H. Vach, J. Häger, and H. Walther, J. Chem. Phys. **90**, 6701 (1989).
[10] Y. Huang, A. M. Wodtke, H. Hou, C. T. Rettner, and D. J. Auerbach, Phys. Rev. Lett. **84**, 2985 (2000).
[11] M. Asscher, W. L. Guthrie, T. H. Lin, and G. A. Somorjai, Phys. Rev. Lett. **49**, 76 (1982).
[12] J. W. Hepburn, F. J. Northrup, G. L. Ogram, J. C. Polyani, and J. M. Williamson, Chem. Phys. Lett. **85**, 127 (1982).
[13] D. A. Mantell, S. B. Ryali, G. L. Haller, and J. B. Fenn, J. Chem. Phys. **78**, 4250 (1983).
[14] D. Ettinger, K. Honma, M. Keil, and J. C. Polyani, Chem. Phys. Lett. **87**, 413 (1982).
[15] K. R. Lykke and B. D. Kay, J. Chem. Phys. **92**, 2614 (1990).
[16] W. Allison and B. Feuerbacher, Phys. Rev. Lett. **45**, 2040 (1980).
[17] J. P. Cowin, C. Yu, S. J. Sibener, and L. Wharton, J. Chem. Phys. **79**, 3537 (1983).
[18] M. Gostein, H. Parhikhteh, and G. O. Sitz, Phys. Rev. Lett. **75**, 342 (1995).
[19] E. Watts, G. O. Sitz, D. A. McCormack, G. J. Kroes, R. A. Olsen, J. A. Groeneveld, J. N. P. Van Stralen, E. J. Baerends, and R. C. Mowrey, J. Chem. Phys. **114**, 495 (2001).
[20] Elizabeth Watts and Greg O. Sitz, J. Chem. Phys. **114**, 4171 (2001).
[21] M. F. Bertino, A. P. Graham, L. Y. Rusin, and J. P. Toennies, J. Chem. Phys. **109**, 8036 (1998).
[22] K. C. Janda, J. E. Hurst, J. Cowin, L. Wharton, and D. J. Auerbach, Surf. Sci. **130**, 395 (1983).
[23] A. K. Kummel, G. O. Sitz, R. N. Zare, and J. C. Tully, J. Chem. Phys. **91**, 5793 (1989).
[24] G. O. Sitz, A. C. Kummel, R. N. Zare, and J. C. Tully, J. Chem. Phys. **89**, 2572 (1988); **89**, 6947 (1988); **91**, 5793 (1989).
[25] G. O. Sitz and R. L. Farrow, J. Chem. Phys. **93**, 7883 (1990).
[26] D. A. Mantell, S. B. Ryali, G. L. Haller, and J. B. Fenn, J. Chem. Phys. **78**, 4250 (1983).
[27] A. Boschetti, A. Cagol, C. Corradi, R. Jacobs, M. Mazzola, and S. Ianotta, Chem. Phys. **163**, 179 (1992).
[28] B. D. Kay, T. D. Raymond, and M. E. Coltrin, Phys. Rev. Lett. **59**, 2792 (1987).
[29] A. C. Wight and R. E. Miller, J. Chem. Phys. **109**, 1976 (1998).
[30] T. W. Francisco, N. Camilone, and R. E. Miller, Phys. Rev. Lett. **77**, 1402 (1996).
[31] T. E. Gough, R. E. Miller, and G. Scoles, Appl. Phys. Lett. **30**, 338 (1977).
[32] A. C. Wight and R. E. Miller, J. Chem. Phys. **109**, 8626 (1998).
[33] A. C. Wight, M. Penno, and R. E. Miller, J. Chem. Phys. **111**, 8622 (1999).
[34] H. Zhang and J. R. Manson, J. Chem. Phys. **113**, 8290 (2000).
[35] J. Dai and J. R. Manson, Nucl. Instrum. Methods Phys. Res. B (to be published).
[36] M. F. Bertino, J. R. Manson, and W. Silvestri, J. Chem. Phys. **108**, 10 239 (1998).
[37] Ileana Iftimia and J. R. Manson, Phys. Rev. B **65,** 125401 (2002).
[38] Ileana Iftimia and J. R. Manson, Phys. Rev. Lett. **87**, 093201 (2001).
[39] R. Brako and D. M. Newns, Phys. Rev. Lett. **48**, 1859 (1982).

[40] R. Brako and D. M. Newns, Surf. Sci. **123**, 439 (1982).
[41] V. Celli, D. Himes, P. Tran, J. P. Toennies, Ch. Wöll, and G. Zhang, Phys. Rev. Lett. **66**, 3160 (1991).
[42] F. Hofmann, J. P. Toennies, and J. R. Manson, J. Chem. Phys. **101**, 10 155 (1994); **106**, 1234 (1997).
[43] J. M. Jackson and N. F. Mott, Proc. R. Soc. London, Ser. A **137**, 703 (1932).
[44] F. O. Goodman and H. Y. Wachman, *Dynamics of Gas-Surface Scattering* (Academic, New York, 1976).
[45] G. W. C. Kaye and T. H. Laby, *Tables of Physical and Chemical Constants and Some Mathematical Functions* (Longman, London, 1986).
[46] G. W. Farnell, in *Physical Acoustics*, edited by W. P. Mason and R. N. Thurston (Academic, New York, 1970), Vol. 6, pp. 106.
[47] G. Brusdeylens, R. B. Doak, and J. P. Toennies, Phys. Rev. B **27**, 3662 (1983).
[48] A. Muis and J. R. Manson, J. Chem. Phys. **107**, 1655 (1997).
[49] J. R. Manson, Phys. Rev. B **58**, 2253 (1998).
[50] A. Muis and J. R. Manson, J. Chem. Phys. **111**, 730 (1999).